Dynamic spin correlations in the frustrated cubic phase of MnV_2O_4

Jae-Ho Chung,[1,*] Young-Sang Song,[1] J.-H. Kim,[2,3] T. Suzuki,[4] T. Katsufuji,[4] M. Matsuda,[5] and S.-H. Lee[3]
[1]*Department of Physics, Korea University, Seoul 136-713, Korea*
[2]*Max-Planck-Institut für Festkörperforschung, Heisenbergstraße 1, 70569 Stuttgart, Germany*
[3]*Department of Physics, University of Virginia, Charlottesville, Virginia 22904, USA*
[4]*Department of Physics, Waseda University, Tokyo 169-8555, Japan*
[5]*Quantum Condensed Matter Division, Oak Ridge National Laboratory, Oak Ridge, Tennessee 37831-6393, USA*
(Received 11 July 2013; published 23 September 2013)

The ferrimagnetic spinel MnV_2O_4 undergoes an orbital-induced cubic-to-tetragonal distortion at $T_{\rm YK} = 58$ K, below which noncollinear commensurate ferrimagnetic ordering occurs. Using inelastic neutron scattering, we investigated low-energy dynamics in its cubic phase above $T_{\rm YK}$. We observed two types of coexisting short-range magnetic excitations: the dispersive spin waves centered around the Brillouin-zone centers, $\mathbf{k}_0 = (0, 0, 0)$, and quasielastic spin fluctuations centered at incommensurate wave vectors, $\mathbf{k}_{\rm incom} = (\xi, \xi, 0)$. The coexistence of the two distinct features can be understood as a dynamic realization of the conical spiral order observed in cubic spinels such as $CoCr_2O_4$.

DOI: 10.1103/PhysRevB.88.094430 PACS number(s): 75.40.Gb, 78.70.Nx, 75.50.Gg

I. INTRODUCTION

Novel states can emerge in magnetic materials when there are competitions between underlying degrees of freedom. A well-known example is the case where the geometry of the lattice prohibits the unique global minimization of the magnetic energy and thereby suppresses conventional antiferromagnetic (AFM) ordering.[1,2] The so-called *geometrically frustrated* systems have large ground-state degeneracy, upon which fluctuating spins tend to reorganize in order to satisfy local magnetic interactions.[3] Nontrivial long-range spin structures can also appear when several distinct exchange interactions with comparable magnitudes coexist and compete with each other. Such complex spin structures can induce novel phenomena, of which magnetoelectric multiferroics is a good example. In multiferroics, novel electric polarization may appear when the inversion symmetry of the spin ordering is broken and allows the spin degree of freedom to couple with the electronic one.[4]

Spinel oxides ($A^{2+}B_2^{3+}O_4^{2-}$) provide a fertile ground to investigate complex magnetic interactions. As shown in Fig. 1(a), the A^{2+} ions form a diamond lattice with two face-centered sublattices, while the B^{3+} ions form a network of corner-shared tetrahedra that is highly frustrating.[5–11] When only the B^{3+} ions are magnetic and have AFM interaction with each other, long-range order becomes suppressed in the cubic phase and local spin fluctuations such as hexagonal clusters can emerge.[7,10] When both sites are occupied by magnetic ions, on the other hand, a series of phase transitions involving complex magnetic structures have been observed.[12–18] Ground-state magnetic structures depend on the relative strengths of the AFM exchanges involved, $u = 4J_{\rm BB}S_{\rm B}/3J_{\rm AB}S_{\rm A}$, where $J_{\rm BB}$ and $J_{\rm AB}$ are the coupling constants for the interaction between B and B, and between A and B, respectively.[12] If both $J_{\rm AB}$ and $J_{\rm BB}$ are antiferromagnetic and $J_{\rm AB}$ is stronger than $J_{\rm BB}$ ($u < 8/9$),[12] then a collinear Néel ferrimagnetic (FIM) ordering gets selected, in which S_A and $S_{\rm B}$ are antiferromagnetically aligned while the $S_{\rm B}$ spins are aligned ferromagnetically with each other. The associated magnetic propagation vector for this ordering is $\mathbf{k}_0 = (0, 0, 0)$ [see Fig. 1(b)]. If $J_{\rm BB}$ is sufficiently large to satisfy $u > 8/9$, on the other hand, the ordering of $S_{\rm B}$ deviates from being collinear as shown in Fig. 1(c). The total energy can be lowered by the noncollinear Yafet-Kittel (YK) ordering,[19] yielding additional magnetic Bragg peaks at $\mathbf{k}_{\rm YK} = (4n + 2,0,0)$ prohibited in the collinear Néel ordering. The additional antiferromagnetic components of the B ions are geometrically frustrated, therefore their long-range ordering is observed only when the crystal symmetry is lowered as evidenced in MnV_2O_4, Mn_3O_4, and Fe_3O_4.[13–15,20] For the cubic lattice, however, a conical spiral structure can be the ground state if $J_{\rm BB}$ is not too large [see Fig. 1(d)]. As a result, an additional set of incommensurate (IC) Bragg peaks with $\mathbf{k}_{\rm incom} = (\xi, \xi, 0)$ coexist with the ferrimagnetic Bragg peaks with $\mathbf{k}_0$. The conical spiral phase was theoretically expected to be stable for $u \lesssim 1.3$,[16] but it has experimentally been observed even for larger u values such as in $CoCr_2O_4$ ($u \approx 2.0$) and $MnCr_2O_4$ ($u \approx 1.5$).[17,18] The rotating part of this incommensurate spin ordering can also produce stable ferroelectric polarization via the spin-current mechanism.[21,22]

A natural question that arises is how the magnetic fluctuations above $T_{\rm N}$ evolve as the system approaches the complex transitions. For instance, upon cooling MnV_2O_4 exhibits two magnetic phase transitions; first below $T_{\rm N}$ the collinear Néel order sets in and upon further cooling below $T_{\rm YK}$ the YK ordering of two magnetic ions occur: Mn^{2+} ($3d^5$, $S_{\rm A} = \frac{5}{2}$) on A and V^{3+} ($3d^2$, $S_{\rm B} = 1$) on B sites.[15,23–26] Motivated by this, we have investigated the magnetic dynamics of MnV_2O_4 in its cubic phase above $T_{\rm YK}$. To our surprise, our results show that the magnetic fluctuations above $T_{\rm YK}$ can be explained by the dynamic short-range version of the conical spin order, rather than the Néel or the YK order.

II. EXPERIMENT

A 1-g high quality single crystal of MnV_2O_4 was grown by floating zone method. The same crystal has previously been used to study spin-wave excitations in the tetragonal phase below $T_{\rm YK}$.[26] For the current work, low-energy inelastic neutron-scattering measurements were performed using two (cold and thermal) triple axis spectrometers. The majority of

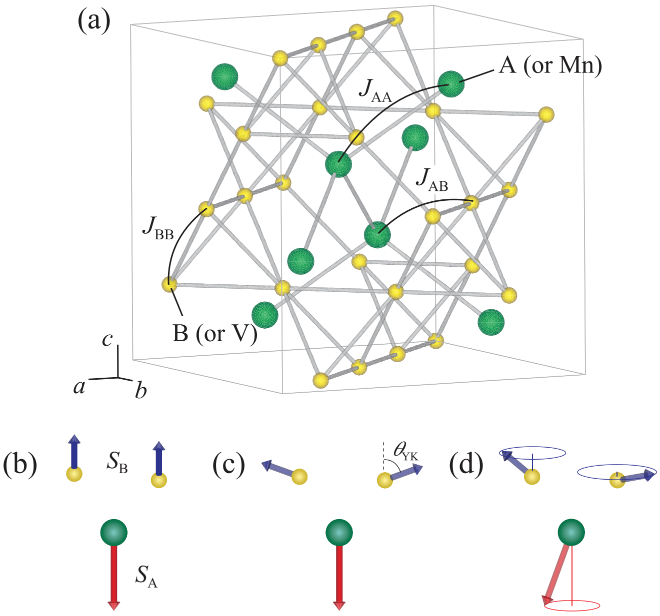

FIG. 1. (Color online) (a) The face-centered-cubic unit cell of AB_2O_4 spinel (or MnV_2O_4). Large and small spheres represent A and B sites, respectively. Bottom: Spin arrangements for (b) collinear Néel, (c) Yafet-Kittel, and (d) conical spiral ferrimagnetic structures. θ_{YK} is the Yafet-Kittel angle.

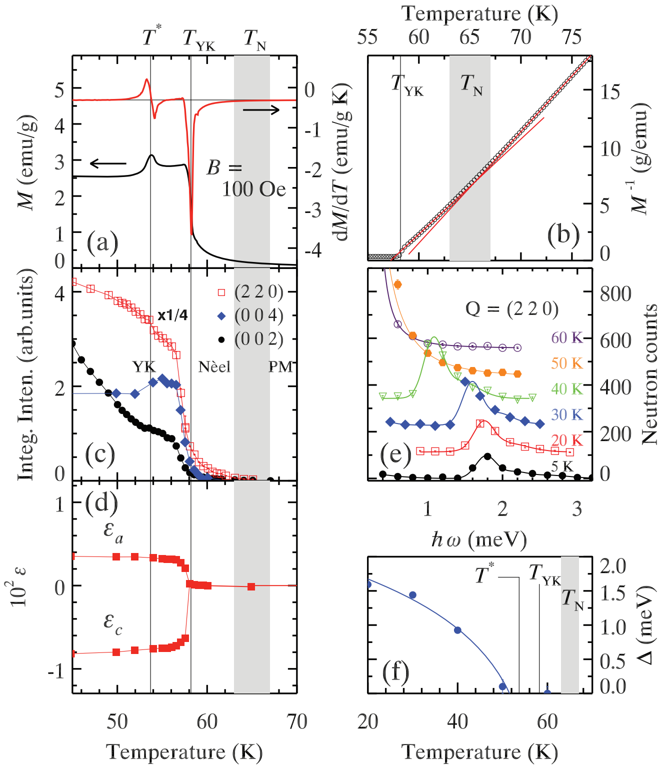

FIG. 2. (Color online) Temperature dependencies of (a) the magnetization and its temperature derivative, (b) inverse magnetization, (c) Bragg peak intensities, and (d) lattice strains, $\varepsilon_l = (l - l_0)/l_0$. The solid lines in (b) are linear fits. In (c), intensities due to nuclear scattering are subtracted. (e) Energy dependence of the low-energy inelastic neutron-scattering spectra measured at $\mathbf{Q} = (2\ 2\ 0)$. (f) Temperature dependence of the spin gap, Δ. The solid curve is a power-law fit.

data were obtained using the SPINS cold neutron spectrometer of the NIST Center for Neutron Research. The analyzer energy was fixed at $E_f = 5.0$ meV, while the incident neutron beam was produced with variable incident energy. Using a pair of 80′ Soller collimators placed before and after the sample, respectively, the energy resolution of ≈ 0.2 meV in full width at half maximum (FWHM) were obtained at the energy transfer of $\hbar\omega = 0.6$ meV. A LN_2-cooled low-pass Be filter ($E \leqslant 5.1$ meV) was inserted in the scattered beam to remove higher-order contaminations. Additional data were collected using the HB1 thermal neutron spectrometer at the High Flux Isotope Reactor facility of the Oak Ridge National Laboratory. The analyzer energy was fixed at $E_f = 12.9$ meV, and the sequence of Soller collimators (48′-40′-40′-120′) were inserted through the beam path providing FWHM ≈ 1.0 meV at $\hbar\omega = 1.0$ meV. Two pyrolytic graphite filters were used to minimize higher-order contaminations.

III. RESULTS AND DISCUSSIONS

A. Review of magnetic phase transitions

Previously two magnetic phase transitions have been reported in MnV_2O_4 at low temperatures: upon cooling, first the paramagnetic (PM) to the collinear Néel phase in the cubic at T_N, and second the collinear Néel to the Yafet-Kittel phase accompanied by a cubic-to-tetragonal distortion at T_{YK}.[15,25–27] The transition at T_N is typically very weak and difficult to identify precisely. An additional anomaly was reported a few degrees below T_{YK}, the nature of which is still controversial.[23–25,27] The exact values of these temperatures varied among different studies, causing some confusion. Overall, single-crystal samples tend to show larger intervals between T_{YK} and T_N. Plumier *et al.* earlier reported $T_{YK} = 53$ K and $T_N = 56$ K using neutron-diffraction and magnetization measurement on a powder sample.[15] Recently Suzuki *et al.* observed the tetragonal distortion at a higher temperature, $T_{YK} = 57$ K, using synchrotron x-ray diffraction of a single crystal.[24] Garlea *et al.* in contrast reported much lower $T_{YK} = 52$ K but higher $T_N \approx 60$ K using single-crystal neutron diffraction.[25] They also reported a large drop of the magnetization well below T_{YK}, which overlapped with neither of the two transitions. Such discrepancies may be due to a possible subtle mixing between Mn and V sites, which requires further experimental studies.

Our dc magnetization and neutron-diffraction results on a single crystal indicate that it is at $T_{YK} = 58$ K where large changes occur in both measurements. Figure 2(a) shows the temperature dependence of the dc magnetization measured using a small piece from the same crystal, for which a weak external field ($B = 100$ Oe) was applied approximately parallel to [111] direction. The sharp peak in dM/dT coincides with the onset of (0 0 2) magnetic Bragg peak and the cubic-to-tetragonal lattice distortion [see Figs. 2(a), 2(c), and 2(d)]. The onset of the collinear Néel ordering, in contrast, is less clear but suspected to be as high as $T_N \approx 65$ K judging from weak enhancements both in magnetization and the diffraction intensities. We also notice a coincidental weak change in slope of the inverse magnetization, which supports the existence of weak magnetic transition [see Fig. 2(b)].

It is also noticeable that there is an additional anomaly a few degrees below T_{YK} in the dc magnetization. Figure 2(a) shows that there is a λ-like feature near 54 K, which we mark as T^*, followed by a noticeable decrease of the magnetization. Similar anomalies have been observed in several previous reports.[23–28] Interestingly, we realize magnetic neutron-diffraction intensities also show possibly associated changes at the same temperature. Figure 2(b) shows that all three Bragg peak intensities commonly exhibit small changes at T^*. Whereas the intensity of (0 0 4) reflection remained constant below T^*, those of (2 2 0) and (0 0 2) continued to increase upon further cooling. It suggests that the YK ordering is further stabilized upon cooling while θ_{YK} continues to change below T^*. The anomaly at T^* has previously been explained to be associated with the enhanced orbital fluctuations.[28,29] Such orbital fluctuations will affect not only the magnetic/orbital ordering but also enhance the magnetocrystalline anisotropy.[25] Figure 2(f) shows that the spin-wave gap appears around T^* and its size increases towards low temperature. It suggests that the orbital order becomes fully locked in only between T^* and T_{YK}.

B. Inelastic neutron scattering

In the cubic phase, above T_{N}, the orbital degrees of freedom of V^{3+} ions are disordered and thus the exchange interactions should be spatially isotropic on average. As a result, the magnetic interactions are strongly frustrated and only dynamic short-range spin correlations may exist. In order to experimentally investigate the dynamic spin correlation, we performed inelastic neutron scattering above T_{YK}.

Figures 3(a) and 3(b) show the inelastic neutron-scattering intensity measured with $\hbar\omega = 0.6$ meV at $T = 65$ K in the $(hk0)$ and the (hkk) scattering plane, respectively. The value of energy transfer, $\hbar\omega = 0.6$ meV, was chosen because it was high enough to minimize contaminations from the strong elastic scattering while the weak quasielastic scattering was still detectable. It is apparent that the observed intensity distribution is clearly different from the case of the chromate spinels with nonmagnetic A-site ions.[7,10] Instead of a broad ringlike distribution that extends beyond one Brillouin zone in the $(hk0)$ plane, a sharper and narrower ring is observed tightly around the wave vector $\mathbf{Q} = (2\,2\,0)$. This can be understood as isotropic spin-wave-like excitations, anticipating the magnetic ordering below T_{N}. Similar excitations have been reported above T_{C} in ferromagnets[30–33] or above T_{N} in antiferromagnets.[34] Interestingly, however, there are additional intensities in Fig. 3 that are anisotropic and uncharacteristic of typical linear spin waves. In the $(hk0)$ plane, the anomalous feature is broadly extended along the $[h\ h\ 0]$ direction exhibiting a distinctive intensity maximum at $h \approx 1.4$. In the (hkk) plane the anomalous feature is present between the two spin-wave-like excitations at around (111) and (022). It is to be noted that no signal was observed around (200).

The appearance of the magnetic signals at the two wave vectors, one commensurate at $\mathbf{k}_0 = (0,0,0)$ and the other incommensurate at $\mathbf{k}_{\mathrm{incom}} = (\xi,\xi,0)$, is reminiscent of the conical spiral phase observed in certain cubic spinels.[12,16,18] In $CoCr_2O_4$ or $MnCr_2O_4$, the two wave vectors account for the axial and the rotating spin components, respectively, of

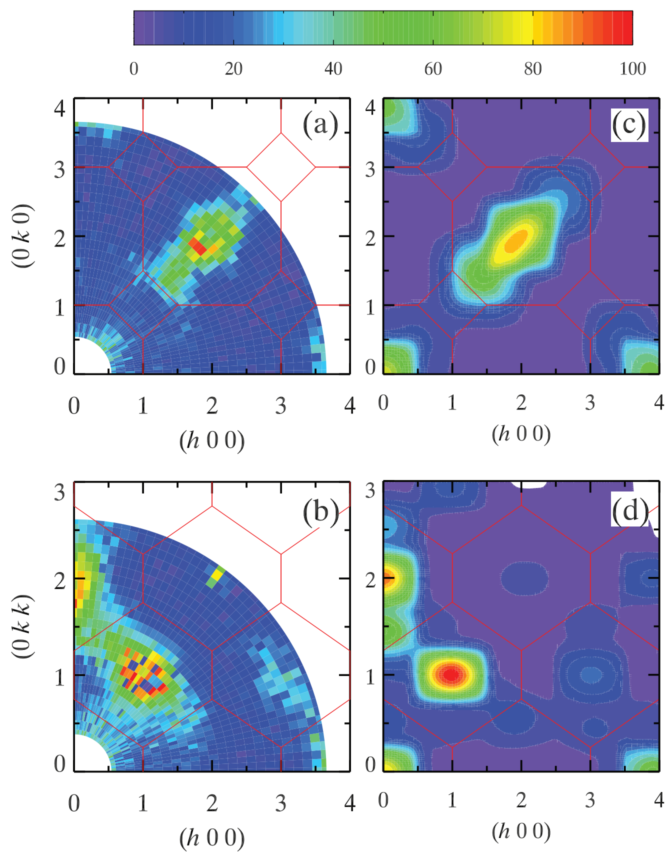

FIG. 3. (Color online) (a), (b) Inelastic neutron-scattering intensity of cubic MnV_2O_4 measured at $\hbar\omega = 0.6$ meV and $T = 65$ K. The red lines mark the Brillouin-zone boundaries. In (b), the sharp signal at $\mathbf{Q} = (2\,2\,2)$ is probably due to a contamination from the (222) nuclear Bragg peak. (c), (d) Neutron-scattering cross sections calculated for the spin correlations obtained from the simulated annealing described in the text ($u = 1.47$).

the static conical spiral ordering. Experimentally they have $u \gtrsim 1.6$, which is higher than the stability limit ($u \approx 1.3$) estimated in theoretical calculations.[12,16] If we assume the exchange interactions in the cubic phase of MnV_2O_4 to be the average value of Js in the tetragonal phase, i.e., $J_{\mathrm{cub}} = \langle J_{\mathrm{tet}}\rangle$, we obtain $u = 1.6 \pm 0.4$, which is similar to the value obtained for the two cubic chromates.

To investigate the two distinct magnetic excitations, we measured the energy dependence of the inelastic neutron-scattering intensity. Figure 4(a) shows several constant-$\hbar\omega$ scans performed along the transverse $\mathbf{Q} = (2 + \xi\ \ 2 - \xi\ \ 0)$ direction. Clearly, only the isotropic spin-wave-like excitations are observed along the transverse direction. It is also clear that the excitations are dispersive; ξ increases as $\hbar\omega$ increases. On the other hand, along the longitudinal $(2 + \xi\ 2 + \xi\ 0)$ direction, there is additional diffusive scattering centered around $\xi \approx 0.6$, that is well separated from the dispersive excitations stemming from (220). The widths of the two excitations are substantially wider than the instrumental resolutions, indicating that they are short ranged.

We have fitted the data with Lorentzians and plotted the results in Fig. 4(c). It is apparent that the diffusive scattering (closed circles) appears more or less at the same wave vector up

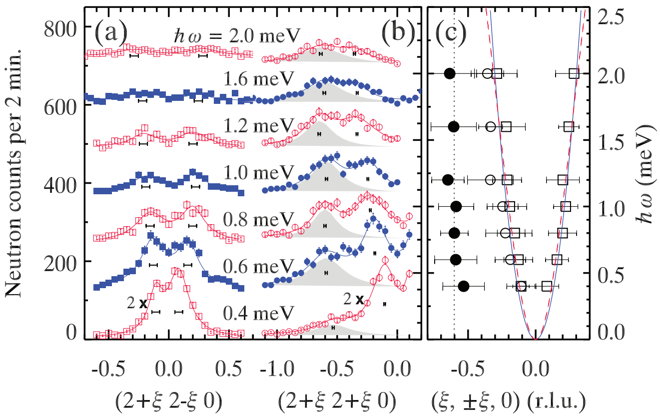

FIG. 4. (Color online) (a), (b) Energy and momentum dependencies of inelastic neutron-scattering intensities measured around $\mathbf{Q} = (2\ 2\ 0)$. The solid lines are Lorentzian fits, and the horizontal bars indicate instrumental resolutions. Shaded areas indicate contributions from the dispersion-less excitation. The fitted peak positions are plotted in (c). The dashed line is the calculated spin-wave dispersion discussed in the text, whereas the solid line is the best-fit curve with $\hbar\omega = D\xi^2$ ($D = 21.31 \pm 0.06$ meV Å^2). The dotted line marks the average wave vector of the dispersionless excitation.

to 2 meV. This indicates that the diffuse scattering is quasielastic in nature, and it is due to local spin fluctuations. In contrast, the spin-wave-like excitations (empty circles and squares) are dispersive, which can be fitted to a ferromagnetic dispersion relation $\hbar\omega = D\xi^2$ (solid line).[35] Within the observed energy range, the spin-wave dispersion also closely resembles the low-energy spin-wave modes observed in other spinels with collinear Néel orderings.[36,37]

Above T_{YK} where the crystal symmetry is cubic, J_{BB} must be frustrated leaving out only the collinear part. When calculating the spin-wave energies in this phase, we thus considered only the collinear component by replacing S_{B} with $S_{\mathrm{B}} \sin\theta_{\mathrm{YK}}$, $\theta_{\mathrm{YK}} = 65^\circ$.[25] The dashed line in Fig. 4(c) shows the low-energy spin-wave mode calculated in this way using $J_{\mathrm{cub}} = \langle J_{\mathrm{tet}} \rangle$ and zero anisotropy.[26]

We also investigated the temperature dependence of the diffusive excitations. Figure 5(a) shows the constant-Q scans measured at $\mathbf{Q} = (1.4\ 1.4\ 0)$ at various temperatures. It is clear that the intensity is absent at 55 K $< T_{\mathrm{YK}}$ but it appears only for $T > T_{\mathrm{YK}}$. The integrated intensity as a function of T, shown in Fig. 5(c), indicates that upon warming it sharply develops and reaches a maximum at T_{YK}. Upon further warming, it stays approximately constant up to T_{N}, and gradually decreases to finally vanish at $T \sim 140$ K. Interestingly, the inverse magnetization also shows a change of slope around this temperature. The difference plots shown in Fig. 5(b) confirms that the incommensurate spin fluctuations are strong between T_{YK} and T_{N}, which is surprising because there is no corresponding static conical spiral order at any temperature. The intensity increase of the incommensurate fluctuations observed at the elastic channel is at most comparable to the inelastic part without any sign of well defined Bragg peaks. Therefore, the observed quasielastic intensities should not be due to thermal excitations of static order, but reflect the fluctuations of the localized spin clusters.

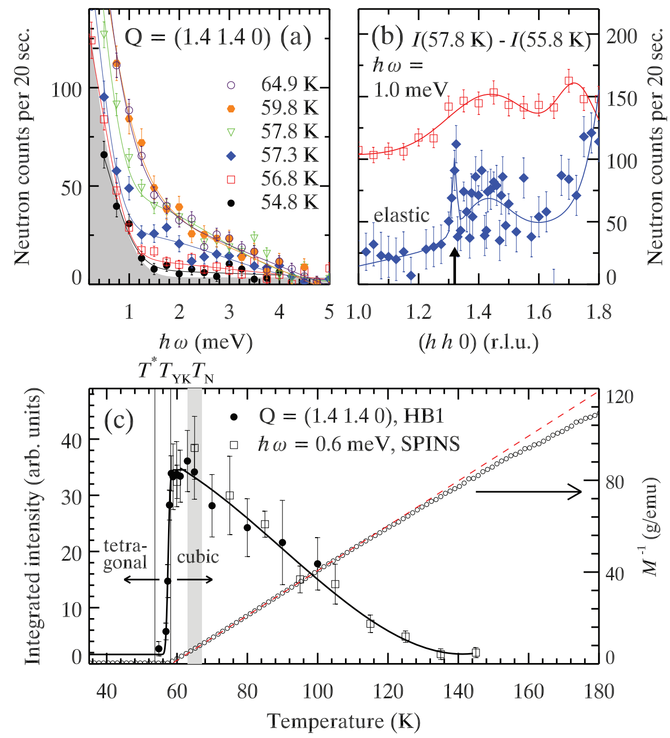

FIG. 5. (Color online) (a) Energy and temperature dependencies of the inelastic neutron-scattering intensities at $\mathbf{Q} = (1.4\ 1.4\ 0)$. The shaded area represents the incoherent background measured at $\mathbf{Q} = (2.5\ 0\ 0)$. The solid lines are guides to the eye. (b) The difference plots of the inelastic and elastic scattering intensities, respectively, between 57.8 and 55.8 K. The data at $\hbar\omega = 1.0$ meV are shifted vertically for clarity. The solid lines are Gaussian fits. The arrow marks the higher-order contamination ($\lambda/3$), which is present at both temperatures. (c) Temperature dependencies of the quasielastic intensity and inverse magnetization. The magnetization was subtracted by the signal from an empty holder before plotting, and the dashed line is the linear fit. The filled circles are obtained by integrating constant-Q scans (1–5 meV), whereas the empty squares are integrated over constant-$\hbar\omega$ scans ($\hbar\omega = 0.6$ meV). The solid line is a guide to the eye.

C. Simulations of neutron-scattering cross sections

In order to understand the nature of the incommensurate spin fluctuations above T_{YK}, we performed simulated annealing and calculated neutron-scattering cross sections for the fluctuating spins in the $4 \times 4 \times 4$ unit cell. The total magnetic energy of $H = \frac{1}{2}\sum_{i \neq j} J_{ij}\mathbf{S}_i \cdot \mathbf{S}_j$ was estimated and minimized for instantaneous dynamic spin configurations to find the optimal configuration using a simulated annealing method. Then, the neutron-scattering intensity was calculated for the optimal dynamic spin configuration by $I(\mathbf{Q}) \sim |F(\mathbf{Q})|^2 = |\sum_j f_j(Q)\mathbf{S}_j \exp(i\mathbf{Q}\cdot\mathbf{r}_j)|^2$ where $f_j(Q)$, $\mathbf{S}_j$, and $\mathbf{r}_j$ are the magnetic form factor, magnetic moment, and the position of the jth spin, respectively.

Some of the results obtained with three different u values are shown in Fig. 6. For $u = 1.6$, the calculation produces strong signals at incommensurate positions along the longitudinal $(\xi,\xi,0)$ direction in the $(hk0)$ plane, which is expected for the conical spiral fluctuations. However, it does not reproduce the spin-wave excitations around the zone centers in either the $(hk0)$ or (hkk) plane [see Figs. 6(a) and 6(b)]. When

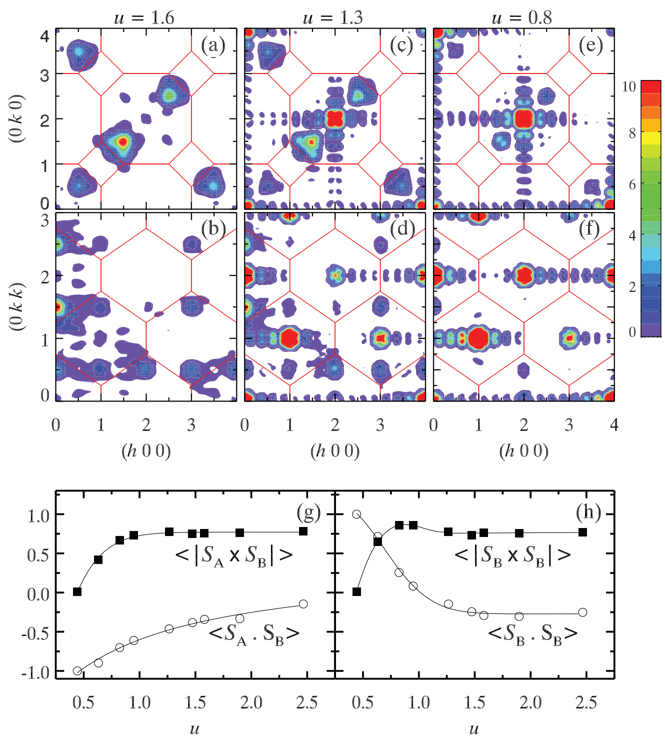

FIG. 6. (Color online) Simulated neutron-scattering cross sections of the spin correlations for (a), (b) $u = 1.6$, (c), (d) $u = 1.3$, and (e), (f) $u = 0.8$, respectively. The white area corresponds to zero intensity. (g), (h) Spin-correlation functions, $\langle|S_i \times S_j|\rangle$ and $\langle S_i \cdot S_j\rangle$ estimated from the simulations, where i and j are the nearest-neighbor A and B ions.

u is decreased, the incommensurate fluctuations weaken, and the spin-wave-like signals appear around the zone centers that are expected for the collinear spin fluctuations [see Figs. 6(c), 6(d), 6(e), and 6(f)]. The competition between the conical spiral and collinear spin fluctuations as a function of u can be seen if we plot the nearest-neighbor spin-correlation functions representing the noncollinearity, $\langle|S_i \times S_j|\rangle$, and the collinearity, $\langle S_i \cdot S_j\rangle$, respectively, as functions of u. As shown in Figs. 6(h) and 6(k), the spin system loses full collinearity when $u \gtrsim 0.5$, where both $\langle|S_A \times S_B|\rangle$ and $\langle|S_B \times S_B|\rangle$ quickly increase. In contrast, $\langle S_B \cdot S_B\rangle$ decreases and eventually changes the sign around $u \sim 1.0$, indicating the enhancement of antiferromagnetic correlation. Its absolute value remains virtually constant beyond $u > 1.5$ due to the strong geometrical frustration. In the meantime, $\langle S_A \cdot S_B\rangle$ continues to approach zero reflecting the gradual loss of collinearity. The overall u dependencies demonstrate that the dynamic correlations evolve from collinear via conical to full frustration with increasing u over the range. As shown in Figs. 6(c) and 6(d), the two features coexist for the intermediate values of u. This tells us that both the conical and the collinear spin fluctuations coexist in the system. The exact value of u cannot be determined, but is estimated to be in the range of $1.3 \lesssim u \lesssim 1.6$.

In order to complete our qualitative comparison of our model to the inelastic data obtained with $\hbar\omega = 0.6$ meV, we calculated the total neutron-scattering cross section from the simulated annealing results. The results are shown in Figs. 3(c) and 3(d), for which the value of $u = 1.47$ was chosen approximately halfway in the range of $1.3 \lesssim u \lesssim 1.6$. Since our model of a finite number of spins cannot reproduce the dispersiveness of the spin-wave excitations, the intensities at Brillouin-zone centers do not exhibit the ring-shaped features but are concentrated to the centers. Reproduction of the ring features would require calculations that can account for time-dependent dynamics. Other than that, the momentum dependence of the intensity distribution qualitatively reproduce the inelastic neutron-scattering data shown in Figs. 3(a) and 3(b).

IV. SUMMARY AND CONCLUSION

In summary, we have observed two distinct features of low-energy spin fluctuations in the geometrically frustrated cubic phase of MnV_2O_4. The dispersionless quasielastic incommensurate fluctuations can be understood as the rotating component of the conical spiral spin correlations, whereas the dispersive spin-wave-like excitations can be accounted for by the spin-wave excitations of the axial component. This dynamic version of the conical spiral ordering is in contrast to the commensurate long-range ordering observed below T_N. Our study tells us that MnV_2O_4 is in the vicinity of a critical point in the phase space where the several distinct phases compete, and the actual ground state is selected by the subtle interplay among the relevant degrees of freedom such as orbital, lattice, and spin.

ACKNOWLEDGMENTS

This work was supported by National Research Foundation of Korea through the ARCNEX (Grant No. 2011-0031933) and the Nuclear R&D Program (Grants No. 2012-025968 and No. 2012-029621). S.H.L. acknowledges support from the US Department of Energy, Basic Energy Research, through Grant No. DE-FG02-07ER46384. We acknowledge the support of the National Institute of Standards and Technology, US Department of Commerce, in providing the neutron research facilities used in this work. Research conducted at ORNL's High Flux Isotope Reactor was sponsored by the Scientific User Facilities Division, Office of Basic Energy Sciences, US Department of Energy.

*jaehc@korea.ac.kr

[1] A. P. Ramirez, Nature (London) **421**, 483 (2003).

[2] *Frustrated Spin Systems*, edited by H. T. Diep (World Scientific, Singapore, 2005).

[3] S.-H. Lee, H. Takagi, D. Louca, M. Matsuda, S. Ji, H. Ueda, Y. Ueda, T. Katsufuji, J.-H. Chung, S. Park, S.-W. Cheong, and C. Broholm, J. Phys. Soc. Jpn. **79**, 011004 (2010).

[4] S.-W. Cheong and M. Mostovoy, Nat. Mater. **6**, 13 (2007).

[5] A. P. Ramirez, A. Hayashi, R. J. Cava, R. Siddharthan, and B. S. Shastry, Nature (London) **399**, 333 (1999).
[6] S.-H. Lee, C. Broholm, T. H. Kim, W. Ratcliff II, and S-W. Cheong, Phys. Rev. Lett. **84**, 3718 (2000).
[7] S.-H. Lee, C. Broholm, W. Ratcliff, G. Gasparovic, Q. Huang, T. H. Kim, and S.-W. Cheong, Nature (London) **418**, 856 (2002).
[8] K. Matsuno, T. Katsufuji, S. Mori, M. Nohara, A. Machida, Y. Moritomo, K. Kato, E. Nishibori, M. Takata, M. Sakata, K. Kitazawa, and H. Takagi, Phys. Rev. Lett. **90**, 096404 (2003).
[9] K. Kamazawa, S. Park, S.-H. Lee, T. J. Sato, and Y. Tsunoda, Phys. Rev. B **70**, 024418 (2004).
[10] J.-H. Chung, M. Matsuda, S.-H. Lee, K. Kakurai, H. Ueda, T. J. Sato, H. Takagi, K.-P. Hong, and S. Park, Phys. Rev. Lett. **95**, 247204 (2005).
[11] M. Matsuda, H. Ueda, A. Kikkawa, Y. Tanaka, K. Katsumata, Y. Narumi, T. Inami, Y. Ueda, and S.-H. Lee, Nat. Phys. **3**, 397 (2007).
[12] D. H. Lyons, T. A. Kaplan, K. Dwight, and N. Menyuk, Phys. Rev. **126**, 540 (1962).
[13] N. Menyuk, K. Dwight, D. Lyons, and T. A. Kaplan, Phys. Rev. **127**, 1983 (1962).
[14] G. B. Jensen and O. V. Nielsen, J. Phys. C: Solid State Phys. **7**, 409 (1974).
[15] R. Plumier and M. Sougi, Solid State Commun. **64**, 53 (1987); Physica B **155**, 315 (1989).
[16] J. M. Hastings and L. M. Corliss, Phys. Rev. **126**, 556 (1962). They reported $u \approx 1.6$ for $MnCr_2O_4$.
[17] N. Menyuk, K. Dwight, and A. Wold, J. Phys. (Paris) **25**, 528 (1964).
[18] K. Tomiyasu, J. Fukunaga, and H. Suzuki, Phys. Rev. B **70**, 214434 (2004).
[19] Y. Yafet and C. Kittel, Phys. Rev. **87**, 290 (1952).
[20] M. S. Senn, J. P. Wright, and J. P. Attfield, Nature (London) **481**, 173 (2012).
[21] H. Katsura, N. Nagaosa, and A. V. Balatsky, Phys. Rev. Lett. **95**, 057205 (2005).
[22] Y. Yamasaki, S. Miyasaka, Y. Kaneko, J.-P. He, T. Arima, and Y. Tokura, Phys. Rev. Lett. **96**, 207204 (2006).
[23] K. Adachi, T. Suzuki, K. Kato, K. Osaka, M. Takata, and T. Katsufuji, Phys. Rev. Lett. **95**, 197202 (2005).
[24] T. Suzuki, M. Katsumura, K. Taniguchi, T. Arima, and T. Katsufuji, Phys. Rev. Lett. **98**, 127203 (2007).
[25] V. O. Garlea, R. Jin, D. Mandrus, B. Roessli, Q. Huang, M. Miller, A. J. Schultz, and S. E. Nagler, Phys. Rev. Lett. **100**, 066404 (2008).
[26] J.-H. Chung, J.-H. Kim, S.-H. Lee, T. J. Sato, T. Suzuki, M. Katsumura, and T. Katsufuji, Phys. Rev. B **77**, 054412 (2008); **87**, 139907(E) (2008).
[27] V. Hardy, Y. Breard, and C. Martin, Phys. Rev. B **78**, 024406 (2008).
[28] K. Myung-Whun, J. S. Kim, T. Katsufuji, and R. K. Kremer, Phys. Rev. B **83**, 024403 (2011).
[29] S. Sarkar, T. Maitra, R. Valentì, and T. Saha-Dasgupta, Phys. Rev. Lett. **102**, 216405 (2009).
[30] H. A. Mook, J. W. Lynn, and R. M. Nicklow, Phys. Rev. Lett. **30**, 556 (1973).
[31] J. W. Lynn, Phys. Rev. B **11**, 2624 (1975).
[32] H. A. Mook and J. W. Lynn, Phys. Rev. Lett. **57**, 150 (1986).
[33] J. W. Cable and R. M. Nicklow, Phys. Rev. B **39**, 11732 (1989).
[34] F. Demmel and T. Chatterji, Phys. Rev. B **76**, 212402 (2007).
[35] T. Izuyama, Phys. Rev. B **5**, 190 (1972).
[36] R. M. Glasser and F. J. Milford, Phys. Rev. **130**, 1783 (1963).
[37] W. Wegener, D. Scheerli, E. Legrand, S. Hautecle, and V. Brabers, Solid State Commun. **15**, 345 (1974).